

Experimental and theoretical investigation of aortic wall tissue in tensile tests

Aleksandra Petuchova^{a,*}, Algirdas Maknickas^{a,b}, Ernest Kostenko^{a,c} and Rimantas Stonkus^d

^a*Department of Biomechanical Engineering, Faculty of Mechanics, Vilnius Gediminas Technical University, Vilnius, Lithuania*

^b*Laboratory of Numerical Simulation, Institute of Mechanics, Faculty of Mechanics, Vilnius Gediminas Technical University, Vilnius, Lithuania*

^c*Veterinary Department, Faculty of Agrotechnology, Vilnius College, Vilnius, Lithuania*

^d*Department of Mechatronics, Robotics and Digital Manufacturing, Vilnius Gediminas Technical University, Vilnius, Lithuania*

Received 27 May 2023

Accepted 6 September 2023

Abstract.

BACKGROUND: Understanding the mechanical properties of aortic tissue is essential for developing numerical computation tools and assessing the risk of aortic aneurysm fractures. Tensile tests using aortic wall specimens allow for the determination of stress and strain depending on the location and direction of the sample.

OBJECTIVE: The aim of this study was to perform a mechanical tensile test using canine aorta samples and create a numerical model of aortic tissue tension from the processed data.

METHODS: Dogbone-shaped samples were dissected from canine aortic segments. The initial measurements were made at zero tension and the tensile tests were conducted at 10 mm/min until rupture. Force and stretch data were used to obtain engineering and true stress-strain curves. The true stress-strain curves were taken until the maximum strength was obtained, after which they were smoothed and fitted using a logistic function with three coefficients. These curves were then used as material mechanical properties for a numerical model of the aortic tissue tension. A simplified rectangle form was used to mimic the middle of the dogbone-shaped portion of the tissue specimen. Experimental displacement data were collected for the boundary conditions of the finite element 3D model.

RESULTS: The experimental data processing revealed that the logistic function described the nonlinear behaviour of the aorta soft tissue with an accuracy of 95% from the start of the tension to the media layer rupture. By applying numerical simulations, we obtained a correspondence of the load curve with an RMSE = 0.069 for the theoretical and experimental external tension data.

CONCLUSION: The numerical investigation confirmed that the non-linear soft tissue was validated by applying a logistic function approach to the mechanical properties of the aortic wall.

Keywords: Aortic wall, mechanical properties, stress-strain curve, tensile test

1. Introduction

According to the European Society of Cardiology, cardiovascular diseases are responsible for 45% of all

*Corresponding author: Aleksandra Petuchova, Department of Biomechanical Engineering, Faculty of Mechanics, Vilnius Gediminas Technical University, Plytinės Str. 25, Vilnius, Lithuania. E-mail: aleksandra.petuchova@vilniustech.lt.

deaths in Europe [1]. These diseases include ruptures and blockages of blood vessels and aortic ruptures, which have a mortality rate of approximately 90% [2] and are often caused by aortic dissection [3], aneurysms [4,5] and atherosclerosis [5,6]. The aorta is the main elastic artery which supplies oxygen-saturated blood to the entire body by expanding in the systole phase and recoiling in the diastole phase. The aortic wall is anatomically divided into three layers: the tunica intima, the tunica media and the tunica adventitia [7]. An understanding of the mechanical properties of the aortic wall is required to develop and improve diagnostic tools and assess rupture risk.

Tensile tests on thoracic aortic tissue can determine the respective mechanical properties in the circumferential and longitudinal directions. Uniaxial tests measure tissue behaviour in one direction [8], while biaxial tests allow simultaneous tensile tests in two directions [9]. The inflation tension test is a biaxial test that is used to simulate loading *in vivo* [10]. These tests allow researchers to assess differences in mechanical properties based on age, location, sample orientation [10] and pathological effects. The most common finding of these studies was increased stiffness and strength in the circumferential direction compared to the axial direction. Histological studies reveal that collagen fibres tend to align in the circumferential direction, suggesting that collagen is involved in tissue strength [11].

The behaviour of the stress-stain curve of the tissues of the aorta can be divided into five different stages: initial elastic modulus stage, physiological elastic modulus stage, maximum elastic modulus stage, yield strength stage and finally ultimate tensile strength [12]. When researchers investigate the mechanical movement of aorta tissues in the physiological elastic modulus stage, they can use polynomial, for example [13], logarithmic, for example [14], exponential [15,16] constitutive laws of aorta tissues or some of the more sophisticated mixtures of them without [17] or with asymmetry [18–20] properties of biological tissues. All these models are developed for modelling of first four stages of stress-strain curve of stretching aorta wall. Therefore, these models can describe good mechanical behaviour of the aortic wall at least in the maximum elastic modulus stage but modelling of the yield strength and the condition of the maximum tensile strength is critical to understanding the process of rupture of the aortic wall.

Animal models such as swine, sheep, primates and large dogs have been used to simulate cardiovascular disease, study pathological occurrence processes and assess treatment and preventive actions [21]. We chose to investigate dog aortic tissue samples because canine models have been established for the study of aortic dissection and aneurysm [22,23].

2. Materials and methods

2.1. Preparation of specimen collection experiment

The aortas (Fig. 1) of two dogs, which were obtained from the Vilnius College Veterinary Clinic, were dissected during their necropsies. The dogs were elderly, 25–30 kg in weight and had been euthanised. The dissected aortic segments were processed and surrounding fat tissues were separated and removed. The tissue samples were stored in saline in a refrigerator at +4°C, saline was replaced every 24 h and tests were performed 72 h after preparation. Longitudinal and circumferential dogbone-shaped [24] samples were dissected from the aortic segments at +22°C prior to the experiment. The initial sample thickness, width and length were measured at zero tension, and the measurements are listed in Table 1.

2.2. Mechanical tensile testing

Tension tests were performed using a Mecmesin MultiTest 2.5-i test machine with an LSC-S 1000N load

Table 1
Specimen measurements at zero tension

Specimen	Width, mm	Sample middle part length, mm	Thickness, mm
LONGB1	13.4	26.7	1.57
LONGB2	12.5	20.7	1.95
LONGB3	15.3	21.4	1.77
LONGS1	16.9	18.7	1.81
LONGS2	15.3	18.9	1.57
CIRCB1	11.8	20	2.47
CIRCB2	13.2	15.7	2.57
CIRCS1	19.4	25	3.13
CIRCS2	15	24.6	2.27

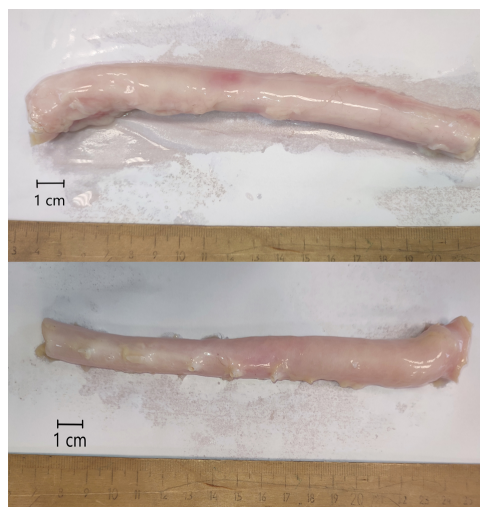


Fig. 1. Two canine aortas obtained from necropsies.

cell (Fig. 2). The force sensor (load sensor measurement error: $\pm 0.1\%$; speed range: 1–1000 mm/min) [25] was conditioned by applying ten 1 N load cycles of 10 mm/min to decrease the effect of relaxation on mechanical response. Tensile tests were conducted at 10 mm/min until rupture [26]. Each test was recorded, and the load (force in N), displacement (range in mm) and time were continuously documented by the data acquisition software. Nine tensile tests were performed with 11 samples as follows: 3 circumferential (CIRCS) and 2 longitudinal (LONGS) from the smaller aorta and 2 circumferential (CIRCB) and 4 longitudinal (LONGB) from the larger aorta (Fig. 3). Each test was filmed to determine the elongation of the middle section from the video footage using graphic processing software. Although eleven specimens were prepared, only nine tensile tests were processed due to tissue spillage or grip breakage.

2.3. Evaluation of the mechanical parameters

Force and stretch data were used to obtain engineering stress and strain curves for each specimen. Data processing was performed using the Matlab 2022b software [27]. Engineering stress was calculated as:

$$\sigma_E = \frac{F}{A_0},$$

where F is the load and A_0 is the initial cross-sectional area before deformation.



Fig. 2. Mecmesin MultiTest 25-i test machine with LSC-S 1000N load cell and camera setup.



Fig. 3. Dog-bone shaped aortic wall samples (scale in cm): A. LONGB, B. CIRCS, C. CIRCB and D. LONGS.

Engineering strain is the amount of material that deforms per unit of length in a tensile test. The engineering strain was calculated as:

$$\varepsilon_E = \frac{\Delta L}{L_0},$$

where ΔL is the change in sample length and L_0 is initial length.

True stress is the applied load divided by the actual cross-sectional area (A) of the material, which changes with time. True strain equals the natural log of the quotient of the current length over the original length for sequential deformations, with consideration of the influence of the deformation path. The assumption of arterial incompressibility implies a zero-volume change, and the true data can be related to the engineering data as follows [8]:

$$A\Delta L = A_0\Delta L_0$$

$$\sigma_T = \frac{F}{A} = \frac{FL}{A_0L_0} = \sigma_E * \frac{L_0 + \Delta L}{L_0} = \sigma_E(1 + \varepsilon_E)$$

$$\varepsilon_T = \int d\varepsilon = \int_{L_0}^L \frac{dL}{L} = \ln \frac{L}{L_0} = \ln \frac{L_0 + \Delta L}{L_0} = \ln(1 + \varepsilon_E)$$

Where σ_T is true stress and ε_T is true strain.

2.4. Curve fitting

Stress-strain curve fitting was performed using the Curve Fitting toolbox of the Matlab software [28]. The curve was fit using the following logistic function with three coefficients:

$$\sigma_T = \frac{L}{1 + e^{-K(\varepsilon_T - A)}}$$

The coefficients were calculated for each sample

2.5. Numerical simulation

Solidworks 2022 [29] software was used to model the tensile test and compare the load force results of the simulated and experimental data. The simplified rectangle form Fig. 3 was used to mimic the middle part of the dogbone-shaped sample. As boundary conditions, the true stress-strain fit curve, Poisson ratio (0.45) [30], material density (1080 kg/m³) [31] and tensile strength of the stress-strain curve were used. The total number of nodes was 50468 and 33031 elements of the 3D model mesh were generated. One end of the 3D model was fixed and tension was applied to the other end. Experimental displacement data were collected at 18 mm for the boundary condition of the 3D finite element model.

2.6. Ethical approval

All animal welfare and bioethical standards adhered to Regulation (EC) No 1069/2009 of the European Parliament and Council of 21 October 2009 and Regulation (EC) No 1774/2002 (Animal by-products Regulation) – 17 articles [32].

3. Results

3.1. Experiment data and results

Nine uniaxial tests were performed using samples taken from the longitudinal ($n = 5$) and circumferential ($n = 4$) directions of the aortic wall. The mean maximum load force to rupture for longitudinal samples was $F_{\max} = 22.88$ N and the maximum tissue displacement was $\Delta l_{\max} = 12.69$ mm, while for the circumferential samples, the respective values were $F_{\max} = 18.9$ N and $\Delta l_{\max} = 27.86$ mm. The longitudinal samples under load elongated 1.6 times until rupture, while the circumferential samples elongated 2 times. The engineering stress-true strain curves shown in Fig. 4 were obtained using measurements before the experiment and data material analyses. The deformation data was taken from the tensile machine data, but we used videographic and photographic material to specify the initial and final length value of the sample after being gripped by the machine. We minimise clamping artefacts during measurements such as material slippage by reducing these deformation (elongation) data value by 10% using measurements from video material. True stress-strain curves were created until the ultimate strength was reached (Fig. 5A). The curves were then smoothed (Fig. 5B) and fitted using a logistic function with three coefficients, which are presented in Table 2. The ultimate tensile strengths under loading conditions were found to be 1.425 ± 0.425 MPa and 1.085 ± 0.235 MPa in the longitudinal and circumferential directions, respectively. The average rupture strains were 0.392 ± 0.09 and 0.78 ± 0.058 for the two directions, respectively.

Table 2
Curve fitting coefficients

Specimen	L	K	A
LONGB1	1.55	21.71	0.2098
LONGB2	1.131	16.6	0.2954
LONGB3	1.764	16.3	0.3059
LONGS1	2.427	11.78	0.3827
LONGS2	1.676	14.64	0.2974
CIRCB1	1.357	8.691	0.63
CIRCB2	1.237	11.29	0.6004
CIRCS1	1.052	10.57	0.64
CIRCS2	1.409	12.05	0.71

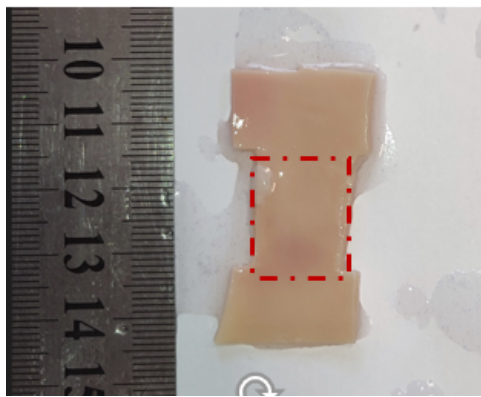


Fig. 4. Simplified rectangle form for numerical simulation.

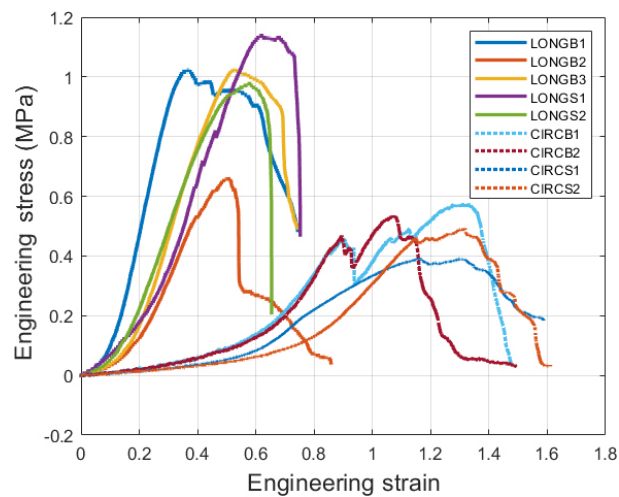


Fig. 5. Engineering stress-strain curves of raw experimental data.

3.2. Simulation results

The results of the calculations are presented graphically using the constructed images. A nonlinear dynamic simulation was performed for a rectangular piece of the aortic wall using measurements obtained

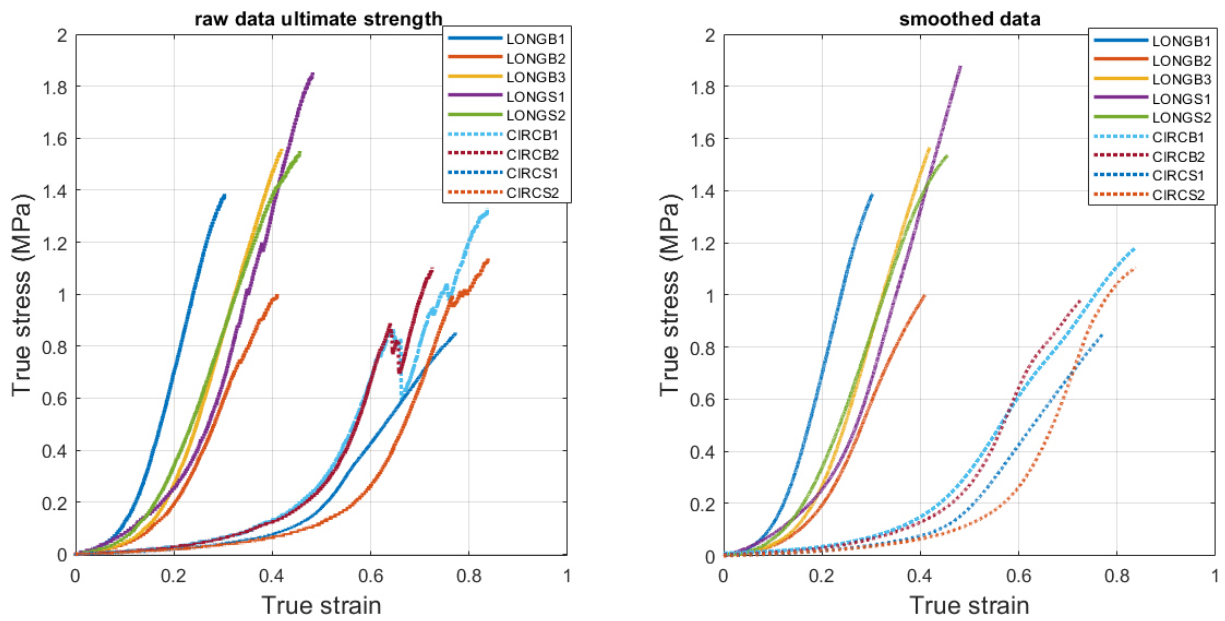


Fig. 6. True stress-strain curves: Right – raw data until ultimate strength, left – smoothed data.

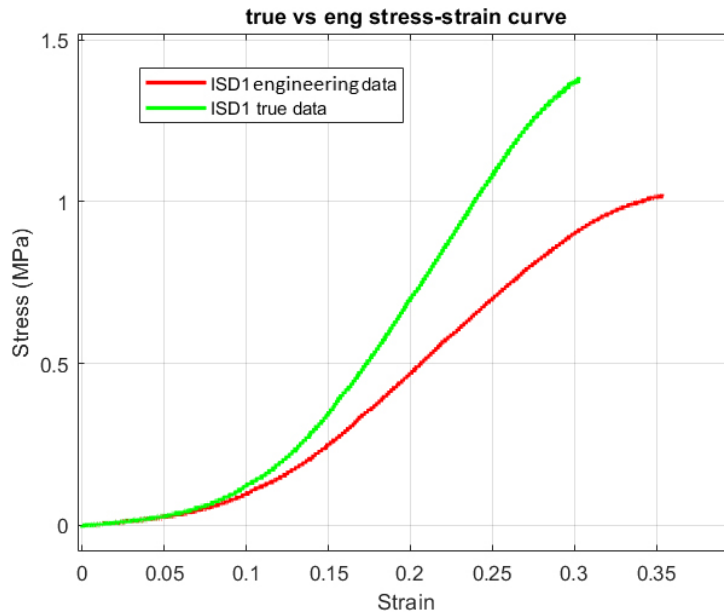


Fig. 7. Engineering and true data comparison of one longitudinal sample.

from the experimental data. During the study, stress and displacement plots were obtained for the aortic wall (Fig. 8A and B). The reaction force was measured at the non-fixed end of the sample and presented as a curve over time compared to the experimental load (Fig. 9). By applying a numerical simulation, we obtained a correspondence of the load curve with an $RMSE = 0.069$ for the theoretical and experimental external tension data.

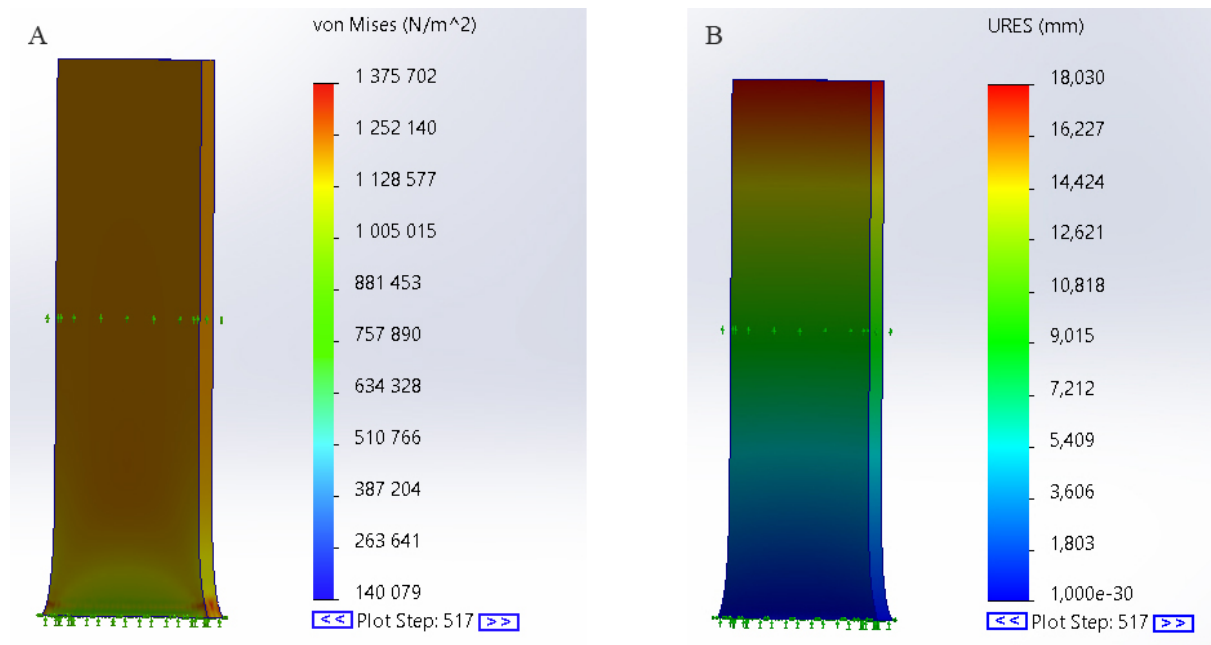


Fig. 8. A. Von Mises stress, B. model displacement during numerical simulation.

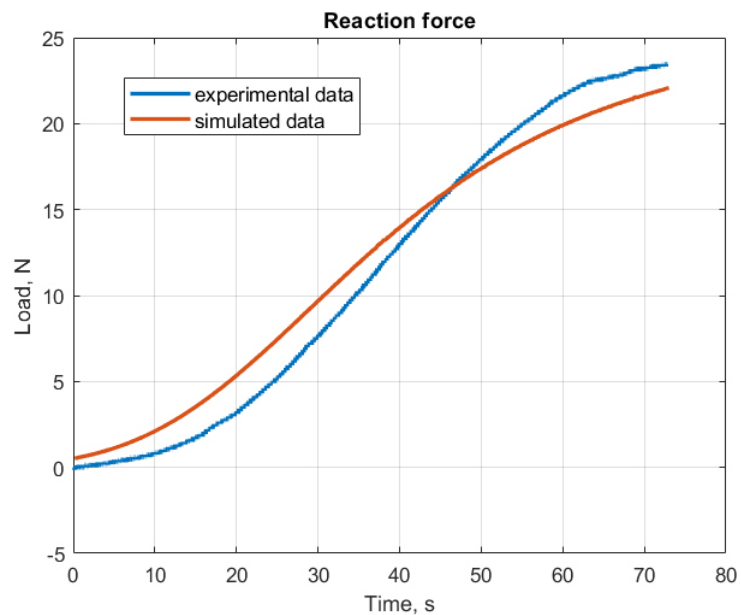


Fig. 9. Reaction load force comparison between experimental data and numerical model.

4. Discussion

This experimental study investigated longitudinal and circumferential deformation through an aortic wall model and evaluated the stress level until rupture by uniaxial tensile testing. Compared to the porcine

aortic tensile test data of the adult pig ultimate tensile strength elastic modulus (9.42 ± 3.32 MPa and 12.33 ± 2.17 MPa for longitudinal and circumferential directions) [33], the adult canine results were 3.5 ± 1.06 MPa and 1.26 ± 0.16 MPa, which indicates a 2.6 times weaker elastic modulus than that of the adult pig in the longitudinal direction and a 9.78 time weaker value in the circumferential samples directions. The failure strain value for the canine samples was 105% and 185% higher than the porcine tissue for the longitudinal and circumferential directions, respectively. Previous studies [34] in porcine aortic tissue data have confirmed that aortic mechanical responses occurred among all aortas, with longitudinal and circumferential stress-to-rupture peaks of 1.4 ± 0.4 MPa and 2.3 ± 0.4 MPa, respectively.

The experimental measurements obtained were then used to fit the material parameters to the known function curve, and the logistic function described the nonlinear behaviour of the aorta soft tissue with an accuracy of 95%. Our fitted curves show the process from the start of tension to the extreme value of a layer, whereas exponential [35], linear [8] or polynomial fittings [10] have stress-strain curve fitting ranges which are smaller.

4.1. Limitations

There were certain limitations of the current study that should be noted. The data presented in this study were obtained using a small number of samples of the canine aortic wall samples; thus, an analysis of variance was performed to estimate the error limits of the properties. Eleven specimens were prepared, but due to severe slippage of the specimens in the metal grips and tears at the gripping point, two datasets were excluded from final analysis. Also, the video recording was made from a single angle which allowed one to track the elongation of the specimen, but did not allow to capture the rupture process of different layers of the aorta from different sides. The limitation of the theoretical simulation was description of the sample material as a whole without separating the aortic wall into layers, i.e. assigning common parameters for the wall, neither assigning to each layer its properties, will give closer results to the real biological material.

We recognise that the use of canine aortas is an important limitation of this study; however, canine aortas were preferred over porcine samples because of the challenges associated with obtaining a sample from an elderly pig that lives an active life. Animal aortas are used regularly in cardiovascular studies [36] because their mechanical properties and structures are comparable to those of humans [37] and samples are more accessible than those of human cadavers.

5. Conclusions

1. An experimental protocol was established. The preparation and storage methods for aortic tissue as well as the equipment used, presentation and processing methods of the results of the tensile experiment were analysed based on the scientific literature.
2. During the experiment, engineering and true stress-strain curves were calculated, and curve fitting was performed using the logistic function with an accuracy of 95%. The processing of tensile experiment data revealed that the maximum stress was greater in the longitudinal than the circumferential direction, whereas strain was higher in the circumferential tensile direction.
3. Validation of the experiment was conducted by the numerical modelling of a nonlinear dynamic problem. The load force curves of the experiment and the numerical model were compared. We obtained a correspondence of the tension force with an $RMSE = 0.069$ for the theoretical and experimental external load force and aorta elongation data.

4. This study shows that the stress-strain curves of aortic tissue can be fitted using a function with three coefficients, thereby providing a detailed description of the non-linearity of the material.

Conflict of interest

None to report.

References

- [1] European Society of Cardiology. CVD in Europe and ESC Congress figures [Internet]. 2019 [cited 2023 Apr 6]. Available from: <https://www.escardio.org/The-ESC/Press-Office/Fact-sheets>.
- [2] Jonker FHW, Verhagen HJM, Lin PH, Heijmen RH, Trimarchi S, Lee WA, et al. Outcomes of endovascular repair of ruptured descending thoracic aortic aneurysms. *Circulation*. 2010 Jun 29; 121(25): 2718-23.
- [3] Rabin A, Palacio D, Saqib N, Bar-Yoseph P, Weiss D, Afifi RO. Aortic aneurysms and dissections: Unmet needs from physicians and engineers perspectives. *J Biomech* [Internet]. 2021; 122: 110461. Available from: doi: 10.1016/j.jbiomech.2021.110461.
- [4] Lavall D, Schäfers HJ, Böhm M, Laufs U. Aneurysms of the ascending aorta. *Dtsch Arztebl Int*. 2012; 109(13): 227-33.
- [5] Ladich E, Yahagi K, Romero ME, Virmani R. Vascular diseases: aortitis, aortic aneurysms, and vascular calcification. Vol. 25, *Cardiovascular Pathology*. Elsevier Inc.; 2016; 432-41.
- [6] Golledge J, Norman PE. Atherosclerosis and abdominal aortic aneurysm: Cause, response, or common risk factors? Vol. 30, *Arteriosclerosis, Thrombosis, and Vascular Biology*. 2010; 1075-7.
- [7] Halushka MK. Genetic Diseases of the Aorta (Including Aneurysms). *Cellular and Molecular Pathobiology of Cardiovascular Disease*. 2014 Jan 1; 239-55.
- [8] Duprey A, Khanafer K, Schlicht M, Avril S, Williams D, Berguer R. *In vitro* characterisation of physiological and maximum elastic modulus of ascending thoracic aortic aneurysms using uniaxial tensile testing. *European Journal of Vascular and Endovascular Surgery*. 2010; 39(6): 700-7.
- [9] Deplano V, Boufi M, Boiron O, Guivier-Curien C, Alimi Y, Bertrand E. Biaxial tensile tests of the porcine ascending aorta. *J Biomech*. 2016 Jul 5; 49(10): 2031-7.
- [10] Ferrara A, Morganti S, Totaro P, Mazzola A, Auricchio F. Human dilated ascending aorta: Mechanical characterization via uniaxial tensile tests. *J Mech Behav Biomed Mater* [Internet]. 2016; 53: 257-71. Available from: doi: 10.1016/j.jmbm.2015.08.021.
- [11] Cebull HL, Rayz VL, Goergen CJ. Recent advances in biomechanical characterization of thoracic aortic aneurysms. *Front Cardiovasc Med*. 2020; 7(May): 1-11.
- [12] Avanzini A, Battini D, Bagozzi L, Bisleri G. Biomechanical evaluation of ascending aortic aneurysms. *Biomed Res Int* [Internet]. 2014 [cited 2023 Aug 28]; 2014. Available from: <https://pubmed.ncbi.nlm.nih.gov/24991568/>.
- [13] Ogden Raymond William. Large deformation isotropic elasticity – on the correlation of theory and experiment for incompressible rubberlike solids. *Proceedings of the Royal Society of London A Mathematical and Physical Sciences* [Internet]. 1972 Feb 1 [cited 2023 Aug 28]; 326(1567): 565-84. Available from: doi: 10.1098/rspa.1972.0026.
- [14] Gent AN. A new constitutive relation for rubber. *Rubber Chemistry and Technology* [Internet]. 1996 Mar 1 [cited 2023 Aug 28]; 69(1): 59-61. Available from: doi: 10.5254/1.3538357.
- [15] Zhou J, Fung YC. The degree of nonlinearity and anisotropy of blood vessel elasticity. *Proc Natl Acad Sci U S A* [Internet]. 1997 Dec 23 [cited 2023 Aug 28]; 94(26): 14255-60. Available from: doi: 10.1073/pnas.94.26.14255.
- [16] Humphrey JD. The Normal Arterial Wall. *Cardiovascular Solid Mechanics* [Internet]. 2002 [cited 2023 Aug 28]; 249-364. Available from: https://link.springer.com/chapter/10.1007/978-0-387-21576-1_7.
- [17] Kas'yanov VA, Rachev AI. Deformation of blood vessels upon stretching, internal pressure, and torsion. *Mechanics of Composite Materials* [Internet]. 1980 Jan [cited 2023 Aug 28]; 16(1): 76-80. Available from: <https://link.springer.com/article/10.1007/BF00618816>.
- [18] Holzapfel GA, Gasser TC, Ogden RW. A new constitutive framework for arterial wall mechanics and a comparative study of material models. *J Elast* [Internet]. 2000 [cited 2023 Aug 28]; 61(1-3): 1-48. Available from: <https://link.springer.com/article/10.1023/A:1010835316564>.
- [19] Holzapfel GA, Sommer G, Gasser CT, Regitnig P. Determination of layer-specific mechanical properties of human coronary arteries with nonatherosclerotic intimal thickening and related constitutive modeling. *Am J Physiol Heart Circ Physiol* [Internet]. 2005 Nov [cited 2023 Aug 28]; 289(5). Available from: <https://pubmed.ncbi.nlm.nih.gov/16006541/>.

- [20] Gasser TC, Ogden RW, Holzapfel GA. Hyperelastic modelling of arterial layers with distributed collagen fibre orientations. *J R Soc Interface* [Internet]. 2006 Feb 22 [cited 2023 Aug 28]; 3(6): 15-35. Available from: <https://pubmed.ncbi.nlm.nih.gov/16849214/>.
- [21] Bianco RW, Wasiluk KR, Voight JM, Lahti MT, Rivard AL, Gallegos RP. CHAPTER II.3.7 LARGE ANIMAL MODELS IN CARDIAC AND VASCULAR BIOMATERIALS RESEARCH AND ASSESSMENT.
- [22] Sénémaud J, Caligiuri G, Etienne H, Delbosc S, Michel JB, Coscas R. Translational relevance and recent advances of animal models of abdominal aortic aneurysm. *Arterioscler Thromb Vasc Biol*. 2017 Mar 1; 37(3): 401-10.
- [23] Li W, Li J, li Q, Cui M, Xu R, Zhai S, et al. A canine model of aortic arch aneurysm created with autologous pericardium. *Journal of Interventional Medicine*. 2022 Aug 1; 5(3): 133-7.
- [24] Pei M, Zou D, Gao Y, Zhang J, Huang P, Wang J, et al. The influence of sample geometry and size on porcine aortic material properties from uniaxial tensile tests using custom-designed tissue cutters, clamps and molds. *PLoS One* [Internet]. 2021; 16(2 February): 1-19. Available from: doi: 10.1371/journal.pone.0244390.
- [25] MultiTest-i Single-column force tester – Mecmesin [Internet]. [cited 2022 May 2]. Available from: <https://www.mecmesin.com/software-controlled-force-systems/single-column-force-tester>.
- [26] Khanafer K, Schlicht MS, Berguer R. How should we measure and report elasticity in aortic tissue? *European Journal of Vascular and Endovascular Surgery*. 2013 Apr; 45(4): 332-9.
- [27] The MathWorks Inc. MATLAB version: 9.13.0 (R2022b) [Internet]. Natick, Massachusetts, United States; 2022 [cited 2023 Apr 11]. Available from: <https://www.mathworks.com>.
- [28] Curve Fitting Toolbox [Internet]. [cited 2023 Apr 11]. Available from: <https://nl.mathworks.com/products/curvefitting.html>.
- [29] SOLIDWORKS Simulation | SOLIDWORKS [Internet]. [cited 2023 May 16]. Available from: <https://www.solidworks.com/product/solidworks-simulation>.
- [30] Di Martino ES, Guadagni G, Fumero A, Ballerini G, Spirito R, Biglioli P, et al. Fluid-structure interaction within realistic three-dimensional models of the aneurysmatic aorta as a guidance to assess the risk of rupture of the aneurysm. *Med Eng Phys*. 2001 Nov 1; 23(9): 647-55.
- [31] Yokawa K, Tsukube T, Yagi N, Hoshino M, Nakashima Y, Nakagawa K, et al. Abstract 490: Quantitative and Dynamic Measurements of Aortic Wall of Acute Type-A Aortic Dissection With X-Ray Phase-Contrast Tomography. *Arterioscler Thromb Vasc Biol*. 2017 May; 37(suppl_1).
- [32] Regulation (EC) No. 1069/2009 of the European Parliament and of the Council laying down health rules as regards animal by-products and derived products not intended for human consumption and repealing Regulation (EC) No. 1774/2002 (Animal by-products Regulation). | FAOLEX [Internet]. [cited 2023 Jun 5]. Available from: <https://www.fao.org/faolex/results/details/en/c/LEX-FAOC091925/>.
- [33] Gaur P, Sharma S, Kumar D, Chawla A, Mukherjee S, Lalwani S, et al. High rate failure properties of porcine aortic tissue under uniaxial tension. Vol. 26, *International Journal of Crashworthiness*. 2021; 109-19.
- [34] Nauta FJH, Conti M, Marconi S, Kamman AV, Alaimo G, Morganti S, et al. An experimental investigation of the impact of thoracic endovascular aortic repair on longitudinal strain. *European Journal of Cardio-thoracic Surgery*. 2016 Nov 1; 50(5): 955-61.
- [35] Xiong J, Wang SM, Zhou W, Wu JG. Measurement and analysis of ultimate mechanical properties, stress-strain curve fit, and elastic modulus formula of human abdominal aortic aneurysm and nonaneurysmal abdominal aorta. *J Vasc Surg*. 2008 Jul; 48(1): 189-95.
- [36] Patelis N, Moris D, Schizas D, Damaskos C, Perrea D, Bakoyiannis C, et al. Animal models in the research of abdominal aortic aneurysms development. *Physiol Res* [Internet]. 2017 [cited 2023 Aug 28]; 66: 899-915. Available from: www.biomed.cas.cz/physiolres.
- [37] Orsi AM, Stefanini MA, Crocci AJ, Simões K, Ribeiro AACM. Some segmental features on the structure of the aortic wall of the dog. *Anat Histol Embryol* [Internet]. 2004 Jun [cited 2023 Aug 28]; 33(3): 131-4. Available from: <https://pubmed.ncbi.nlm.nih.gov/15144278/>.